Synthesis and Preclinical Evaluation of Three Novel Fluorine-18 Labeled Radiopharmaceuticals for P-Glycoprotein PET Imaging at the Blood−Brain Barrier

Heli Savolainen,[†] Mariangela Cantore,[‡,§] Nicola A. Colabufo,[‡,§] Philip H. Elsinga,[†] Albert D. Windhorst,[‖] and Gert Luurtsema*[,†]

[†]Department of Nuclear Medicine and Molecular Imaging, University of Groningen, University Medical Center Groningen, Hanzeplein 1, 9713 GZ Groningen, Netherlands

[‡]Dipartimento di Farmacia-Scienze del Farmaco, Università degli Studi di Bari, via Orabona 4, 70125 Bari, Italy

[§]Biofordrug slr, via Orabona 4, 70125 Bari, Italy

[‖]Department of Radiology and Nuclear Medicine, VU University Medical Center Amsterdam, De Boelelaan 1085 C, 1081 HV Amsterdam, Netherlands

ABSTRACT: P-Glycoprotein (P-gp), along with other transporter proteins at the blood−brain barrier (BBB), limits the entry of many pharmaceuticals into the brain. Altered P-gp function has been found in several neurological diseases. To study the P-gp function, many positron emission tomography (PET) radiopharmaceuticals have been developed. Most P-gp radiopharmaceuticals are labeled with carbon-11, while labeling with fluorine-18 would increase their applicability due to longer half-life. Here we present the synthesis and *in vivo* evaluation of three novel fluorine-18 labeled radiopharmaceuticals: 4-((6,7-dimethoxy-3,4-dihydroisoquinolin-2(1*H*)-yl)methyl)-2-(4-fluorophenyl)oxazole (**1a**), 2-biphenyl-4-yl-2-fluoroethoxy-6,7-dimethoxy-1,2,3,4-tetrahydro-isoquinoline (**2**), and 5-(1-(2-fluoroethoxy))-[3-(6,7-dimethoxy-3,4-dihydro-1*H*-isoquinolin-2-yl)-propyl]-5,6,7,8-tetrahydronaphthalen (**3**). Compounds were characterized as P-gp substrates *in vitro*, and *Mdr1a/b*$^{(−/−)}$*Bcrp1*$^{(−/−)}$ and wild-type mice were used to assess the substrate potential *in vivo*. Comparison was made to (*R*)-[^{11}C]verapamil, which is currently the most frequently used P-gp substrate. Compound [^{18}F]**3** was performing the best out of the new radiopharmaceuticals; it had 2-fold higher brain uptake in the *Mdr1a/b*$^{(−/−)}$*Bcrp1*$^{(−/−)}$ mice compared to wild-type and was metabolically quite stable. In the plasma, 69% of the parent compound was intact after 45 min and 96% in the brain. Selectivity of [^{18}F]**3** to P-gp was tested by comparing the uptake in *Mdr1a/b*$^{(−/−)}$ mice to uptake in *Mdr1a/b*$^{(−/−)}$*Bcrp1*$^{(−/−)}$ mice, which was statistically not significantly different. Hence, [^{18}F]**3** was found to be selective for P-gp and is a promising new radiopharmaceutical for P-gp PET imaging at the BBB.

KEYWORDS: blood−brain barrier, P-glycoprotein, BCRP, PET, ^{18}F, radiopharmaceutical
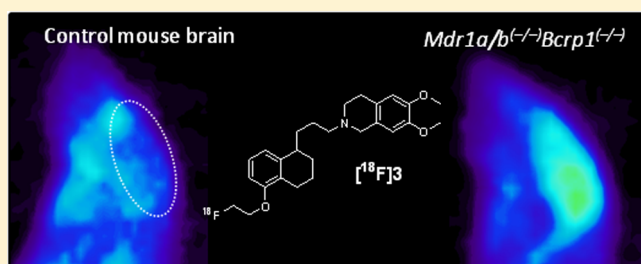
1. INTRODUCTION

P-Glycoprotein (P-gp) is an efflux transporter protein on the luminal membrane of the brain endothelial cells.[1] It belongs to a family of transporters that has a similar function at the blood−brain barrier (BBB), where P-gp and the Breast Cancer Resistance Protein (BCRP) are the most important in the human brain.[2] This family of transporters is also known as the ATP-binding cassette (ABC) transporters, as their function is ATP dependent.[3] They recognize small hydrophobic exogenous compounds that have diffused through the BBB and efflux them back into the blood. Consequently, P-gp not only protects the brain from harmful compounds, but can also reduce the uptake of drugs that need to act in the brain.[4] Moreover, P-gp function is altered in some neurological diseases. For instance, decreased P-gp function has been found in Alzheimer's disease (AD)[5,6] and Parkinson's disease

(PD),[7] while it has been hypothesized that P-gp function is increased in epilepsy.[8]

Positron emission tomography (PET) is a molecular imaging technique that is able to measure tissue concentrations of compounds labeled with positron emitting isotopes as a function of time in a noninvasive manner. To study P-gp function with PET, radiolabeled substrates as well as radiolabeled inhibitors could be applied.[9] The most widely used substrate radiopharmaceutical for P-gp imaging is [^{11}C]-verapamil. It has been used either as racemic mixture or as (*R*)-enantiomer[10] and has been utilized in clinical research.[11,12] The P-gp inhibitors [^{11}C]tariquidar and [^{11}C]elacridar were

Chart 1. Structures of $[^{18}F]1a$, $[^{18}F]2$, $[^{18}F]3$, $[^{18}F]$Fluoroethyl Tariquidar, $[^{18}F]$Fluoroethyl Elacridar and 1-$[^{18}F]$Fluoroelacridar

[^{18}F]1a

[^{18}F]2

[^{18}F]3

[^{18}F]fluoroethyl tariquidar

[^{18}F]fluoroethyl elacridar: R1=CH$_2$CH$_2$^{18}F, R2=H
1-[^{18}F]fluoroelacridar: R1=CH$_3$, R2=^{18}F
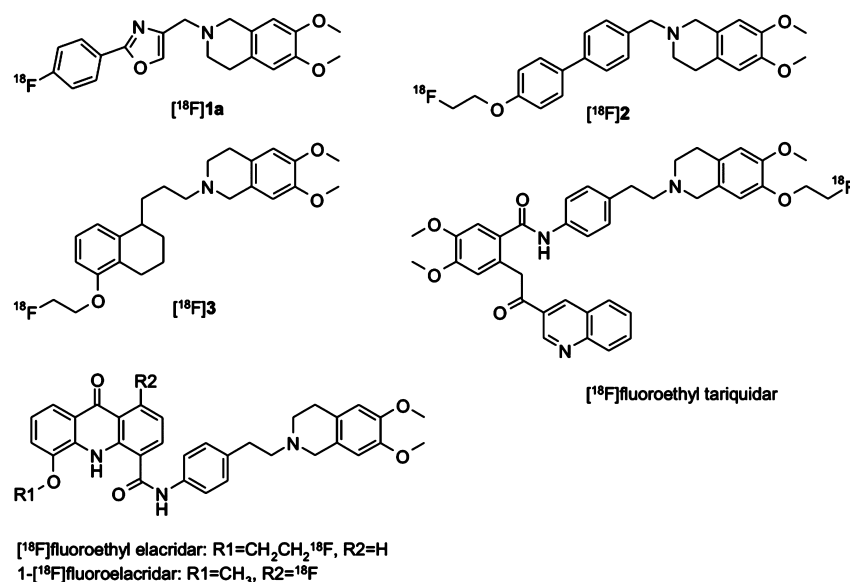
aimed to bind P-gp with high selectivity. However, they were proved to behave as substrates at tracer level and are not specific for P-gp, but are also transported by BCRP.[13,14]

Most of the labeled compounds that are currently in use are labeled with carbon-11, while labeling with fluorine-18 would lead to a radiopharmaceutical that can be transported to other imaging centers without on-site cyclotron due to the longer half-life of fluorine-18 of 110 min vs 20 min for carbon-11. In addition, the longer half-life would enable prolonged imaging times and also more subjects could be dosed from one radiopharmaceutical production. Half-life of fluorine-18 can be a disadvantage only if repeated scanning for the same subject during one day is desired.

There are only a few examples of fluorine-18 labeled P-gp radiopharmaceuticals that have been applied in CNS disorders. Tariquidar and elacridar analogues have been labeled with fluorine-18 by a fluoroalkylation method, demonstrating similar *in vivo* behavior as their carbon-11 labeled counterparts.[15] An elacridar analogue has been labeled also via a nucleophilic aromatic fluorination, but the utilization of 1-$[^{18}F]$-fluoroelacridar is limited due to the low radiochemical yield and *in vivo* defluorination.[16]

Clearly, there is an unmet need to develop ^{18}F-radiolabeled compounds to study P-gp function with PET at the BBB. We report three novel compounds: 4-((6,7-dimethoxy-3,4-dihydroisoquinolin-2(1H)-yl)methyl)-2-(4-fluorophenyl)oxazole (**1a**), 2-biphenyl-4-yl-2-fluoroethoxy-6,7-dimethoxy-1,2,3,4-tetrahydro-isoquinoline (**2**), and 5-(1-(2-fluoroethoxy))-[3-(6,7-dimethoxy-3,4-dihydro-1H-isoquinolin-2-yl)-propyl]-5,6,7,8-tetrahydronaphthalen (**3**), which were identified as P-gp substrates in *in vitro* experiments, as presented in this Article. All of the compounds contain the same basic 6,7-dimethoxytetrahydroisoquinoline moiety as tariquidar or elacridar also have.[17,18] All three compounds were labeled with fluorine-18 (Chart 1), and their brain uptake was investigated with PET imaging in FVB mice as well as in the $Mdr1a/b^{(-/-)}Bcrp1^{(-/-)}$ knockout mice, and results were compared to those of (R)-$[^{11}C]$verapamil. In addition, $[^{18}F]3$ was investigated in $Mdr1a/b^{(-/-)}$ mice to see if the compound was selective for P-gp.

2. EXPERIMENTAL SECTION

2.1. Chemicals and Cell Lines. All reagents and solvents were obtained from commercial suppliers (Merck (New Jersey, USA), Sigma-Aldrich (St. Louis, USA), Rathburn (Walkerburn, UK), and B. Braun (Melsungen, Germany)) and were used without further purification. (R)-Norverapamil was purchased from ABX advanced biochemical compounds (Radeberg, Germany). Human liver microsomes were obtained from BD Gentest (20 mg/mL) (San Jose, USA). Cell culture reagents were purchased from Celbio s.r.l. (Pero Mi, Italy). CulturePlate 96/wells plates were bought from PerkinElmer Life Science (Waltham, USA). MDCK-MDR1, MDCK-BCRP, and MDCK-MRP1 cell lines were a gift from Professor P. Borst, NKI-AVL Institute, Amsterdam, Netherlands. Caco-2 cells were a gift from Dr. Aldo Cavallini and Dr. Caterina Messa from the Laboratory of Biochemistry, National Institute for Digestive Diseases, 'S. de Bellis', Bari, Italy.

2.2. Organic Synthesis. *2.2.1. General Methods.* Column chromatography was performed with Merck silica gel 60 Å (63−200 μm) as the stationary phase. Recording of mass spectra was done on an HP 6890-5973MSD gas chromatograph/mass spectrometer (Santa Clara, USA); only significant m/z peaks, with their percentage of relative intensity in parentheses, are reported. ^{1}H NMR spectra were recorded in CDCl$_3$ at 300 MHz with Varian Mercury-VX spectrometer (Palo Alto, USA) or on an Avance 500 MHz spectrometer (Bruker, Billerica, USA). All chemical shift values are reported in ppm (δ) relative to the solvent peak (7.27 for CHCl$_3$). Melting points were determined in open capillary on a Gallenkamp electrothermal apparatus (Leicestershire, UK). ESI-MS analyses were performed on an Agilent 1100 LC/MSD trap system VL (Santa Clara, USA). Elemental analyses (C, H, N) were performed on Eurovector Euro EA 3000 analyzer (Milan, Italy); the analytical results were within ±0.4% of the theoretical values for the given formula.

2.2.2. Synthesis of 4-Fluorobenzamide (5a). 4-Fluorobenzoic acid (**4a**, 2.0 g, 14 mmol) was refluxed with SOCl$_2$ (2.0 mL, 28 mmol) in the presence of Et$_3$N (1.0 mL, 7.2 mmol) for 1 h. After evaporation of SOCl$_2$, the resulting acyl chloride was

added to a 45 mL mixture of NH_4OH (8 M), H_2O, and CH_2Cl_2 (1:1:1 v/v/v). This mixture was stirred at room temperature for 4 h. The organic layer was separated from the aqueous layer and washed with 2 M NaOH (3 × 10 mL). The organic solution was dried over Na_2SO_4 and evaporated under reduced pressure. The residue was purified by silica gel column chromatography (CH_2Cl_2/MeOH 95:5 v/v). The yield of brown solid **5a** was 590 mg (30%). GC−MS m/z: 139 (M^+, 67), 123 (100), 95 (72).

2.2.3. Synthesis of 4-(Chloromethyl)-2-(4-fluorophenyl)-oxazole (6a). Amide **5a** (590 mg, 4.2 mmol) was reacted with 1,3-dichloroacetone (1.0 g, 8.4 mmol) at 200 °C for 5 h. After cooling to room temperature, water (10 mL) and $CHCl_3$ (10 mL) were added. The aqueous phase was extracted with $CHCl_3$ (3 × 50 mL), and the combined organic layers were dried over Na_2SO_4 and evaporated under reduced pressure. The residue was purified on silica gel column chromatography (hexane/ EtOAc 8:2 v/v) yielding 270 mg (30%) of **6a** as a brown solid. GC−MS m/z: 213 (M^+ + 2, 19), 211 (M^+, 57), 176 (78). ^{1}H NMR (300 MHz, $CDCl_3$) δ: 8.06 (d, 1H, J = 8.0 Hz, phenyl-H_2), 8.03 (d, 1H, J = 8.1 Hz, phenyl-H_3), 7.60 (s, 1H, oxazole-H_5), 7.18 (d, 1H, J = 8.3 Hz, phenyl-H_6), 7.16 (d, 1H, J = 8.0 Hz, phenyl-H_5), 4.32 (s, 2H, CH_2).

2.2.4. Synthesis of 4-((6,7-Dimethoxy-3,4-dihydroisoqui-nolin-2(1H)-yl)methyl)-2-(4-fluorophenyl)oxazole (1a). Compound **6a** (260 mg, 1.0 mmol) was alkylated with 6,7-dimethoxy-1,2,3,4-tetrahydroisoquinoline (460 mg, 2.4 mmol) in DMF (20 mL) using Na_2CO_3 as a base (250 mg, 2.4 mmol). The mixture was refluxed overnight. DMF was evaporated under reduced pressure, and the residue was partitioned between H_2O (20 mL) and $CHCl_3$ (20 mL). The organic phase was separated, the aqueous phase was extracted with $CHCl_3$ (3 × 50 mL), and the collected organic fractions were dried over Na_2SO_4 and evaporated under reduced pressure. The residue was purified on silica gel column chromatography (CH_2Cl_2/ EtOAc 1:1 v/v) to obtain 270 mg of **1a** as a brown oil in 74% yield. Hydrochloride salt was dissolved in methanol while heating, Et_2O was added, and the solution was cooled down to recrystallize the product. Mp: 232−235 °C. ESI^+/MS m/z: 369 $[M + H]^+$, 391 $[M + Na]^+$. ESI^+/MS/MS m/z: 352 (16), 230 (50), 176 (98), 121 (100). ^{1}H NMR (300 MHz, $CDCl_3$) δ: 8.05 (d, 1H, J = 8.0 Hz, phenyl-H_2) 8.03 (d, 1H, J = 8.1 Hz, phenyl-H_3), 7.60 (s, 1H, oxazole-H_5), 7.16 (d, 1H, J = 8.0 Hz, phenyl-H_5), 7.15 (d, 1H, J = 8.2 Hz, phenyl-H_6), 6.58 (s, 1H, isoquinoline-H_5), 6.50 (s, 1H, isoquinoline-H_8), 3.88 (s, 3H, CH_3), 3.82 (s, 3H, CH_3), 3.75−3.79 (m, 4H, NCH_2CH_2), 2.94 (s, 4H, CH_2NCH_2). Purity of the final compound was established by combustion analysis of the corresponding hydrochloride salt, confirming a purity ≥95%. (C,N,H) $C_{21}H_{21}FN_2O_3HCl(H_2O)_{0.5}$.

2.2.5. Synthesis of 2-Biphenyl-4-yl-2-fluoroethoxy-6,7-dimethoxy-1,2,3,4-tetrahydro-isoquinoline (2). A suspension of NaH (24 mg, 1.0 mmol) in dry DMF (3.0 mL) was stirred at room temperature for 10 min. A solution of phenol precursor **9** (1.0 g, 1.0 mmol) in DMF (1.0 mL) was added, and the solution was stirred for 1 h. A solution of 2-fluoroethyl tosylate was added (860 mg, 2.0 mmol) in DMF (1.0 mL), and the reaction mixture was stirred for 4 h. Water was added until effervescence ceased. The solvent was evaporated, and the residue was partitioned between H_2O (20 mL) and $CHCl_3$ (20 mL). The organic phase was separated, the aqueous phase was extracted with $CHCl_3$ (3 × 50 mL), and the collected organic fractions were dried over Na_2SO_4 and evaporated under

reduced pressure. The residue was purified on silica gel column chromatography ($CHCl_3$/MeOH 19:1 v/v) and recrystallized from MeOH/Et_2O to obtain 190 mg of **2** (45%). (C,N,H) $C_{26}H_{28}FNO_3HCl$. ESI^+/MS m/z: 444 $[M + Na]^+$. ESI^+/MS/ MS m/z: 441 (100). ^{1}H NMR (300 MHz, $CDCl_3$) δ: 7.42 (dd, 4H, J = 7.2 Hz, J = 8.0 Hz phenyl-$H_{2',3',5',6'}$), 7.12 (d, 2H, J = 8 Hz, phenyl-$H_{2,6}$), 7.01 (d, 2H, J = 7.5 Hz, phenyl-$H_{3,5}$), 6.60 (s, 1H, isoquinoline-H_5), 6.45 (s, 1H, isoquinoline-H_8), 4.83 (t, 1H, J = 3 Hz, FCH_2CH_2), 4.60 (t, 1H, J = 3 Hz, FCH_2CH_2), 4.14 (t, 1H, J = 3 Hz, FCH_2CH_2), 4.10 (t, 1H, J = 3 Hz, FCH_2CH_2), 3.83 (s, 3H, CH_3), 3.80 (s, 3H, CH_3), 3.71 (s, 2H, NCH_2), 3.57 (s, 2H, NCH_2) 2.83−2.76 (m, 4H, NCH_2CH_2).

2.2.6. Synthesis of 5-(1-(2-Fluoroethoxy))-[3-(6,7-dime-thoxy-3,4-dihydro-1H-isoquinolin-2-yl)-propyl]-5,6,7,8-tetra-hydronaphthalen (3). A suspension of NaH (48 mg, 2.0 mmol) in dry DMF (3.0 mL) was stirred at room temperature for 10 min. A solution of phenol precursor **14** (560 mg, 2.0 mmol) in DMF (1.0 mL) was added, and the solution was stirred for 1 h. A solution of 2-fluoroethyl tosylate was added (1.1 g, 4.0 mmol) in DMF (1.0 mL), and the reaction mixture was stirred for 4 h. Water was added until effervescence ceased. The solvent was evaporated, and the residue was partitioned between H_2O (20 mL) and $CHCl_3$ (20 mL). The organic phase was separated, the aqueous phase was extracted with $CHCl_3$ (3 × 50 mL), and the collected organic fractions were dried over Na_2SO_4 and evaporated under reduced pressure. The residue was purified on silica gel column chromatography ($CHCl_3$/ MeOH 19:1 v/v) and recrystallized from MeOH/Et_2O to yield 320 mg of **3** (38%). (C,N,H) $C_{26}H_{35}FNO_3HCl$. ESI^+/MS m/z: 450 $[M + Na]^+$. ESI^+/MS/MS m/z: 420 (47), 388 (100). ^{1}H NMR (300 MHz, $CDCl_3$) δ: 7.08 (dd, 1H, J = 7.8 Hz, J = 6 Hz, phenyl-H_7), 6.82 (d, 1H, J = 7.7 Hz, phenyl-H_6), 6.63 (d, 1H, J = 7 Hz, phenyl-H_8), 6.58 (s, 1H, isoquinoline-H_5), 6.50 (s, 1H, isoquinoline-H_8), 4.83 (t, 1H, J = 3 Hz, FCH_2CH_2), 4.66 (t, 1H, J = 3 Hz, FCH_2CH_2), 4.24 (t, 1H, J = 3 Hz, FCH_2CH_2), 4.14 (t, 1H, J = 3 Hz, FCH_2CH_2), 3.84 (s, 3H, CH_3), 3.83 (s, 3H, CH_3), 3.55 (s, 2H, NCH_2), 2.60−2.84 (m, 9H, tetrahydronaphthalen-$CH_2CH_2CH_2CH$, isoquinoline-$NCH_2CH_2CH_2$, NCH_2CH_2), 1.63−1.85 (m, 8H, tetrahydro-naphthalen-$CH_2CH_2CH_2CH$, isoquinoline-$NCH_2CH_2CH_2$).

2.2.7. Synthesis of 2-Fluoroethyl Tosylate. Synthesis of 2-fluoroethyl tosylate was performed by making a solution of 2-fluoroethanol (1.3 mL, 2.0 mmol) and p-toluenesulfonyl chloride (170 mg, 1.1 mmol) in 5 M NaOH (5.0 mL, 1.6 mmol), which was stirred at room temperature for 24 h. The reaction mixture was diluted with CH_2Cl_2, and the organic phase was washed with 10% NaOH. The organic layer was dried (Na_2SO_4) and evaporated under reduced pressure. The crude product was purified by chromatography on a silica gel column with CH_2Cl_2 to give 220 mg (92%) of colorless oil that was stored in a freezer. ESI^+/MS m/z: 241 $[M + Na]^+$. ESI^+/ MS/MS m/z: 241 (74), 97 (100). ^{1}H NMR (300 MHz, $CDCl_3$) δ: 7.80 (d, 2H, J = 8 Hz, phenyl-$H_{2,6}$), 7.34 (d, 2H, J = 8 Hz, phenyl-$H_{3,5}$), 4.49 (t, 1H, J = 4 Hz, CH_2), 4.64 (t, 1H, J = 4 Hz, CH_2), 4.30 (t, 1H, J = 4 Hz, CH_2), 4.21 (t, 1H, J = 4 Hz, CH_2), 2.45 (s, 3H, CH_3).

2.2.8. Synthesis of 2-Bromoethyl Tosylate (15). A volume of 3.0 mL of DCM was added to toluenesulfonyl chloride (950 mg, 5.0 mmol) in a round-bottom flask, and the mixture was brought to 0 °C. Triethylamine (680 μL, 5.0 mmol) was added, and 2-bromoethanol (280 μL, 4.0 mmol) was added dropwise. The mixture was stirred for 1 h at 0 °C. It was brought to room temperature, washed with water (10 mL), brine (10 mL), and

dried over Na_2SO_4. Crude product was concentrated under reduced pressure into brown liquid. Product was purified by silica gel column chromatography (hexane/EtOAc 9:1 v/v). Product was isolated as a colorless liquid (550 mg, yield 49%). ^1H NMR (500 MHz, $CDCl_3$) δ: 7.84 (d, 2H, $J = 5$ Hz, phenyl-$H_{2,6}$), 7.39 (d, 2H, $J = 10$ Hz, phenyl-$H_{3,5}$), 4.31 (t, 2H, $J = 5$ Hz, CH_2), 3.50 (t, 2H, $J = 7$ Hz, CH_2), 2.48 (s, 3H, CH_3).

2.3. Radiochemistry.

2.3.1. Production and Workup of Fluorine-18. $[^{18}F]$Fluoride was produced by irradiation of $[^{18}O]$water with the Scanditronix MC-17 cyclotron (Uppsala, Sweden) via the $^{18}O(p,n)^{18}F$ nuclear reaction. The $[^{18}O]$water containing the $[^{18}F]$fluoride was passed over a pretreated Sep-Pak light Accell Plus QMA (Waters, Milford, USA) (pretreated with 5 mL of 1.4% Na_2CO_3 solution (B. Braun, Melsungen, Germany), washed with water until pH was neutral, and dried using argon). The $[^{18}F]$fluoride was eluted from the cartridge with solution of K_2CO_3 (5.0 mg, 36 mmol in production of $[^{18}F]$1a, and 3.0 mg, 22 mmol in production of $[^{18}F]$2 and $[^{18}F]$3 in 1.0 mL of water) and collected into a vial containing Kryptofix[2.2.2] (15 mg, 40.0 mmol). A volume of 1 mL of dry acetonitrile was added, and solvents were evaporated to dryness at 130 °C with a helium flow (200 mL/min). Next, 0.5 mL of acetonitrile was added, and the mixture was dried again under the same conditions. This procedure was repeated another two times.

2.3.2. Radiosynthesis of $[^{18}F]$1a. The precursor 1b (2.0 mg, 5.0 mmol) was dissolved in 0.5 mL of DMF and was added to the dried $K[^{18}F]F$/Kryptofix complex. Mixture was reacted for 30 min at 160 °C and cooled for 2 min after which 0.5 mL of HPLC eluent (0.05 M NaOAc/MeOH/THF 55:27:18 v/v/v) was added. The total mixture was filtered through an Acrodisc syringe filter (0.4 μm, Pall Life Sciences, Port Washington, USA) and subjected to HPLC purification utilizing a Symmetryshield RPS 5 μm 7.8 × 300 mm column (Waters, Milford, USA) at a flow of 2 mL/min (UV detection at 254 nm, $R_t([^{18}F]$1a) = 15 min). The product was collected into a bottle containing 80 mL of sterile water. After mixing with helium, the solution was passed over an Oasis HLB 1 cm^3 (30 mg) extraction cartridge (Waters, Milford, USA) to trap $[^{18}F]$1a, after which the cartridge was washed twice with 8 mL of water. Finally the product was eluted from the cartridge with 1 mL of ethanol and passed through a Millipore Millex LG filter (0.2 μm, Billerica, USA). The filtrate was diluted with 4 mL of 0.9% NaCl. Analysis of the product was performed by HPLC using an Xterra C18 5 μm 4.6 × 250 mm column (Waters, Milford, USA) and 0.05 M NaH_2PO_4/MeOH/THF 55:27:18 (v/v/v) as eluent at a flow of 1 mL/min.

2.3.3. Radiosynthesis of $[^{18}F]$2 and $[^{18}F]$3. In the synthesis of $[^{18}F]$2 and $[^{18}F]$3, 15 μL (21 mg, 75 μmol) of 2-bromoethyl tosylate (15) in 1.0 mL of 1,2-dichlorobenzene (DCB) was added to the dried fluoride complex. Distillation of the formed $[^{18}F]$bromoethyl fluoride (16) at 90° was started immediately with a helium gas flow (40 mL/min) to the second vial in room temperature containing 2.0 mg of precursor (5.0 mmol 9 or 14) and 3.0 mg (75 mmol) of 60% dispersion of NaH in mineral oil in 0.5 mL of DMF. After 15 min of distillation, vial 2 was reacted for 5 min at 80 °C in the synthesis of $[^{18}F]$3 and 10 min in the synthesis of $[^{18}F]$2. After completion of the reaction, 0.5 mL of HPLC eluent (0.1 M NaOAc/MeCN 5.5:4.5 v/v) was added. The mixture was filtered through an Acrodisc syringe filter (0.4 μm) and subjected to HPLC purification utilizing a Symmetryshield RPS 5 μm 7.8 × 300 mm column at a flow of 3 mL/min (UV detection at 254 nm, R_t of both $[^{18}F]$2 and $[^{18}F]$

3 10 min). The product was collected into a bottle containing 80 mL of sterile water. After mixing with helium, the solution was passed over an Oasis HLB 1 cm^3 (30 mg) extraction cartridge to trap the product, after which the cartridge was washed twice with 8 mL of water. Finally the product was eluted from the cartridge with 1 mL of ethanol and passed through a Millipore Millex LG filter (0.2 μm). The filtrate was diluted with 4 mL of 0.9% NaCl. Analysis of the product was performed by HPLC using an Alltech Alltima C18 5 μm 4.6 × 250 mm as a column (Thermo Fisher Scientific, Waltham, USA) using the same eluent as in prep. HPLC for $[^{18}F]$2 and MeCN/water 1:1 + 0.1% TFA (v/v) for $[^{18}F]$3, both at a flow of 1 mL/min.

2.3.4. Radiosynthesis of (R)-$[^{11}C]$Verapamil. The synthesis of (R)-$[^{11}C]$verapamil was performed as described previously with some modifications.[19] Briefly, $[^{11}C]CH_4$, produced directly in the target using $^{14}N(p,\alpha)^{11}C$ nuclear reaction, was trapped in the liquid nitrogen. $[^{11}C]$Methane was first converted into $[^{11}C]$methyl iodide and further into $[^{11}C]$-methyl triflate by passage through a silver triflate/α-alumina column (Sigma-Aldrich, St. Louis, USA).[19] $[^{11}C]$Methyl triflate was bubbled into (R)-norverapamil (0.5 mg, 1.0 mmol) solution in 0.5 mL of acetonitrile. The reaction mixture was heated for 5 min at 120 °C. Water (0.5 mL) and MeCN (0.5 mL) were added, and the solution was injected into preparative HPLC system (column Symmetryshield RPS 5 μm 7.8 × 300 mm) and purified with 25 mM NaH_2PO_4 pH 7.0/MeCN/MeOH (41:37:22 v/v/v) as mobile phase (flow rate 5 mL/min, UV detection at 210 nm, $R_t((R)$-$[^{11}C]$verapamil) = 9 min). The eluted fraction containing $[^{11}C]$verapamil was collected into 80 mL of sterile water. After mixing with helium, organic solvents were removed by passing the mixture through an Oasis HLB 1 cm^3 (30 mg) extraction cartridge, following rinsing of the cartridge (twice) with 8 mL of saline solution (0.9% NaCl). (R)-$[^{11}C]$Verapamil was eluted by passing 0.8 mL of EtOH through the cartridge and Millipore Millex LG filter (0.2 μm) and formulated with 4 mL of saline solution. Analysis of the product was performed by HPLC using an Alltima C18 5 μm 4.6 × 250 mm column and 0.1 M NaH_2PO_4 (pH 3)/MeCN (65:35 v/v) as eluent (flow rate 1.5 mL/min, UV detection at 210 nm).

2.4. Distribution Coefficient Log D.

n-Octanol (0.5 mL) and phosphate buffered saline (PBS, pH = 7.2, 0.5 mL) were pipetted in 1:1 ratio into Eppendorf tubes. The radio-pharmaceutical solution (~1 MBq, 100 μL) was added, and tubes were vortexed for 1 min and centrifuged for 5 min at 6000 rpm. Samples (100 μL) of octanol and PBS layer were counted on a γ-counter (LKBG-Compugamma CS 1282, Wallac, Waltham, USA). The distribution coefficient log D was calculated as $\log(A_{octanol}/A_{PBS})$. Measurements were done in triplicate.

2.5. Animals.

All animal studies were in compliance with the local ethical guidelines, and protocols were approved by the Institutional Animal Care and Use Committee of the University of Groningen. Male FVB wild type mice (28 ± 1.8 g), *Mdr1a/b$^{(-/-)}$Bcrp1$^{(-/-)}$* constitutive knockout mice (29 ± 1.1 g), and *Mdr1a/b$^{(-/-)}$* constitutive knockout mice (28 ± 2.3 g) developed from the FVB line were purchased from Taconic (Hudson, USA). After arrival, animals were acclimatized at least 7 days in the Central Animal Facility of the University Medical Center Groningen. Mice had access to food and water *ad libitum* and were kept under a 12 h light−dark cycle. During

Scheme 1. Synthesis of 1a,b[a]

a: R = F
b: R = NO$_2$
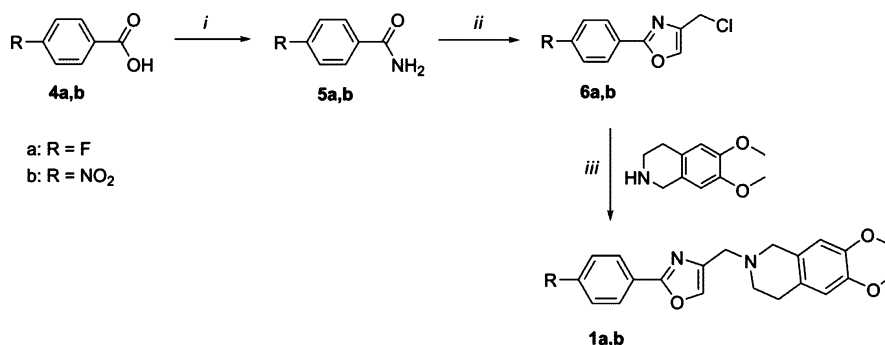
[a]Reagents and conditions: (*i*) SOCl$_2$, Et$_3$N, NH$_4$OH, CH$_2$Cl$_2$; (*ii*) 1,3-dichloroacetone; (*iii*) Na$_2$CO$_3$, DMF.

experiments, mice were anesthetized with 2% isoflurane in medical air and warmed with a heating pad.

2.6. PET Procedure. Mice were injected with a fluorine-18 radiopharmaceuticals (5.3 ± 1.9 MBq, 0.1–0.2 mL, 64 ± 22 ng of **1a**, 7.0 ± 7.0 ng of **2**, 0.3 ± 0.01 ng of **3**) or (*R*)-[^{11}C]verapamil (7.3 ± 3.2 MBq, 0.2 mL, 200 ± 180 ng of verapamil) in the penile vein under isoflurane anesthesia. [^{18}F]**1a** was injected, and animals were transferred into the microPET camera (microPET Focus 220, Siemens Medical Solutions, Malvern, USA) causing a few minutes delay between injection and start of a 60 min dynamic emission scan. All the other radiopharmaceuticals were injected directly on the camera following the start of a 30 min dynamic emission scan. A transmission scan of 515 s with a ^{57}Co point source was performed for correction of attenuation and scatter by tissue after an emission scan. Mice were terminated by cervical dislocation. Several organs and tissues were excised and weighed, and radioactivity was measured with a γ-counter. Radioactivity accumulation in the organs was expressed as standardized uptake value (SUV), using the following formula: [tissue activity concentration (MBq/g)]/[injected dose (MBq)/body weight (g)].

2.7. Metabolite Analysis. *In vitro* metabolism was examined in human liver microsomes. A solution (4.0 mM, 14 μL) of **1a**, **2**, **3**, or (*R*)-verapamil in DMSO was pipetted into test tubes to a final concentration of 20.0 μM. Verapamil was used as a reference compound to check if the microsomes were working adequately because its metabolic pathways are known.[20] PBS (2.6 mL) and human liver microsomes (70.0 μL, final protein concentration 0.5 mg/mL) were added, and tubes were preincubated at 37 °C for 5 min. NADPH solution (20.0 mM, 140 μL) was freshly made in PBS and was added to tubes in final concentration of 1 mM to start the reaction, as NADPH is a cofactor for cytochrome P450 enzymes. The first sample (400 μL) was taken immediately, and proteins were precipitated by addition of acetonitrile + 0.1% formic acid (800 μL). Other samples were taken at time points 15, 30, 45, 60, 90, and 120 min. Three control tubes were also incubated for 120 min: one without microsomes, one without NADPH, and one without test compound. In these tubes the volume of a missing component was replaced by PBS. Sample tubes were vortexed and centrifuged for 6 min at 12000 rpm. Supernatants were analyzed by Xevo QTof UPLC/MS/MS system (Waters, Milford, USA), mounted with ACQUITY UPLC BEH C18 1.7 μm column, H$_2$O/CH$_3$CN + 0.1% HCOOH as eluent at a flow of 0.6 mL/min, ESI positive mode. Metabolynx XS 4.1 software (Waters, Milford, USA) was used for the analysis of

metabolites. Found mass peaks were integrated, and the area was converted to percentage considering the parent area at T = 0 min as 100%. Percentage of the parent compound and found metabolites were expressed as a function of time. Results from 2–3 experiments were fitted using second order polynomial fitting in GraphPad Prism 5 software (La Jolla, USA).

Metabolites formed during the *in vivo* experiments were analyzed from the plasma and brain tissue. Terminal arterial whole blood samples (0.5 mL) were taken after the scans, and they were centrifuged for 5 min at 6000 rpm to obtain plasma. Plasma samples were precipitated by 2 volume addition of acetonitrile and centrifuged, and 2.5–10 μL samples of supernatant were applied on a thin layer chromatography (TLC) plate (F-254 silica gel plates, Sigma-Aldrich, St. Louis, USA). Metabolism in the brain was investigated by dissecting half of the brain and homogenizing it with 0.9 mL of acetonitrile. Brain homogenate was centrifuged, and supernatant was applied on TLC. Plates were eluted with ethyl acetate and methanol, ratio (v/v) 95:5 for [^{18}F]**1a** and [^{18}F]**3** and ratio 99:1 for [^{18}F]**2** (R_f[^{18}F]**1a** = 0.57, R_f[^{18}F]**2** = 0.69, R_f[^{18}F]**3** = 0.41). Radioactivity of the eluted plates was analyzed by phosphor storage imaging. Exposed screens were scanned with a Cyclone phosphor storage system (PerkinElmer Life and Analytical Science, Waltham, USA). Percentage of the intact radiopharmaceutical and the formed metabolites were calculated by region of interest (ROI) analysis using OptiQuant 03.00 software (PerkinElmer, Waltham, USA).

2.8. PET Data Analysis. A 60 min scan, used for [^{18}F]**1a**, was separated into 21 time frames: 6 × 10, 4 × 30, 2 × 60, 1 × 120, 1 × 180, 4 × 300, and 3 × 600 s. A 30 min scan used for other radiopharmaceuticals consequently had the first 18 time frames. Emission sinograms were normalized and corrected for attenuation and radioactive decay. The sinograms were iteratively reconstructed (two-dimensional ordered subsets expectation maximization (OSEM2D) with Fourier rebinning, 4 iterations, and 16 subsets). The final data set consisted of 95 slices with a slice thickness of 0.8 mm and an in-plane image matrix of 128 × 128 pixels. The voxel size was 0.9 mm × 0.9 mm × 0.8 mm. The Inveon Research Workplace software version 4.0 (Siemens) was used for the data analysis. All the frames were summed, and a PET image was coregistered with an MRI template.[21] Whole brain volume of interest (VOI) based on the MRI template was generated. Radioactivity concentration was converted to SUV values and plotted as a time–activity curve (TAC).

2.9. Statistical Analysis. Differences between control (FVB) and knockout animals were calculated for statistical

Scheme 2. Synthesis of 2[a]
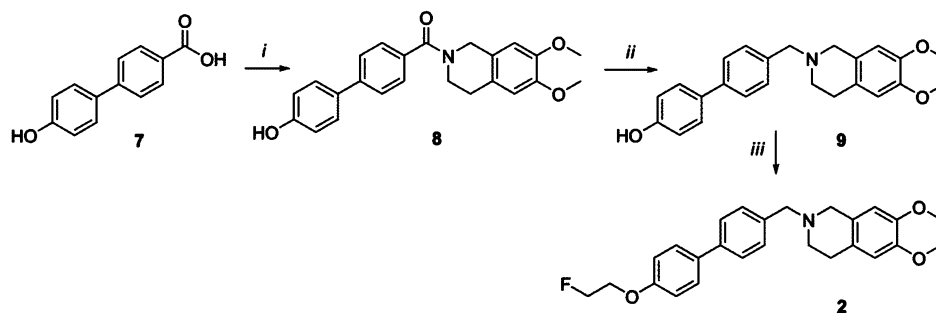
[a]Reagents and conditions: (i) SOCl$_2$ and Et$_3$N; CH$_2$Cl$_2$ and 1.2% NaOH; 6,7-dimethoxytetrahydroisoquinoline; (ii) LiAlH$_4$, THF; (iii) 2-fluoroethyl tosylate, NaH, DMF.

Scheme 3. Synthesis of 3[a]
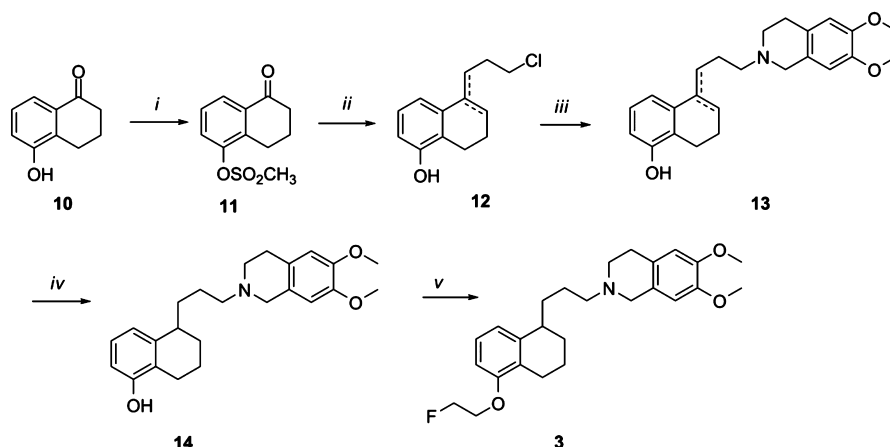
[a]Reagents and conditions: (i) CH$_3$SO$_2$Cl, Et$_3$N, CH$_2$Cl$_2$, T = −10 °C; (ii) cyclopropylmagnesium bromide, 3 N HCl, THF; (iii) 6,7-dimethoxy-1,2,3,4-tetrahydroisoquinoline, Na$_2$CO$_3$, DMF; (iv) H$_2$, Pd/C (5%); (v) 2-fluoroethyl tosylate, NaH, DMF.

Table 1. Results of the Cell Experiments with Nonradioactive Compounds

compd	P$_{app}$ BA/AB	P-gp EC$_{50}$ (μM)	Bcrp EC$_{50}$ (μM)	Mrp1 EC$_{50}$ (μM)	ATPase activation	sigma-1 K_i (nM)	sigma-2 K_i (nM)
1a	9.5	2.1	15	>100	yes	>1000 (35%)	>1000 (25%)
2	7.9	0.54	>100	>100	yes	>1000 (28%)	>1000 (38%)
3	6.1	0.35	>100	>100	yes	>1000 (40%)	>1000 (44%)

significance using either one way analysis of variance (ANOVA) with Bonferroni correction or two-sided unpaired Student's t test. A p-value of less than 0.05 was considered statistically significant. IBM SPSS Statistics version 22 (Armonk, USA) was used for the analysis.

3. RESULTS

3.1. Organic Synthesis. Compounds **1a**, **2**, and **3** were synthesized as displayed in Schemes 1, 2, and 3, respectively. Synthesis of compounds **1b**, **4b**−**6b**, and **7**−**14** has been reported previously, and spectral data of these compounds were identical to those previously described.[17,22,23] Synthesis of compound **1a** was performed in the same conditions as the nitro derivative **1b**. The key intermediate, chloromethyloxazole **6a**, was obtained by cyclization of fluorobenzamide **5a** with dichloroacetone. Compound **1a** was obtained in a high yield (74%) by condensation of **6a** with 6,7-dimethoxytetrahydroisoquinoline. In the synthesis of fluoroethyl compounds **2** and **3**, different approaches were attempted. First, phenol precursors were alkylated with bromoethanol. The resulting hydroxyethyl

compounds were transformed into mesylate or tosylate derivatives. The leaving group was attempted to substitute with fluoride by employing different reagents (NaF, tetrabutylammonium fluoride), but unfortunately the reaction was unsuccessful. Then, as a second approach, fluoroethyl tosylate was prepared by reaction of fluoroethanol with toluensulphonyl chloride. Phenol precursor was reacted with the fluoroethyl tosylate in the presence of different bases (NaOH, KOH, NaH) and solvents (toluene, DMF). Phenol precursors had low reactivity and required the use of NaH and DMF for successful synthesis.

3.2. Cell Experiments. Three different cell experiments were performed with the nonradioactive compounds to examine the substrate potential: apparent permeability experiment in Caco-2 cells, Calcein-AM assay to determine selectively the potency (EC$_{50}$) toward each transporter, and ATP depletion assay. The experimental setup is described in detail elsewhere.[18,24] A compound is defined as a substrate when it is transported, and it activates ATPase. The ratio of drug transport through Caco-2 monolayers in the basolateral-apical
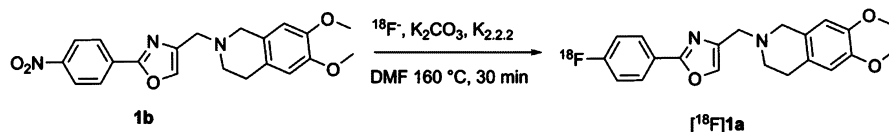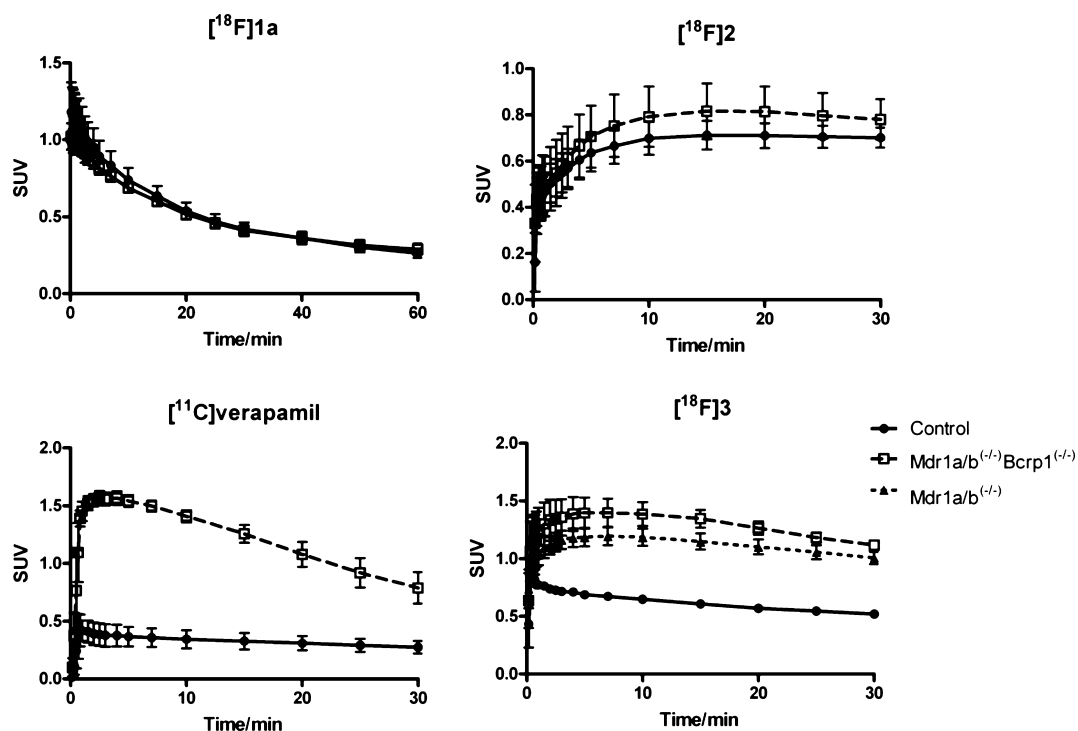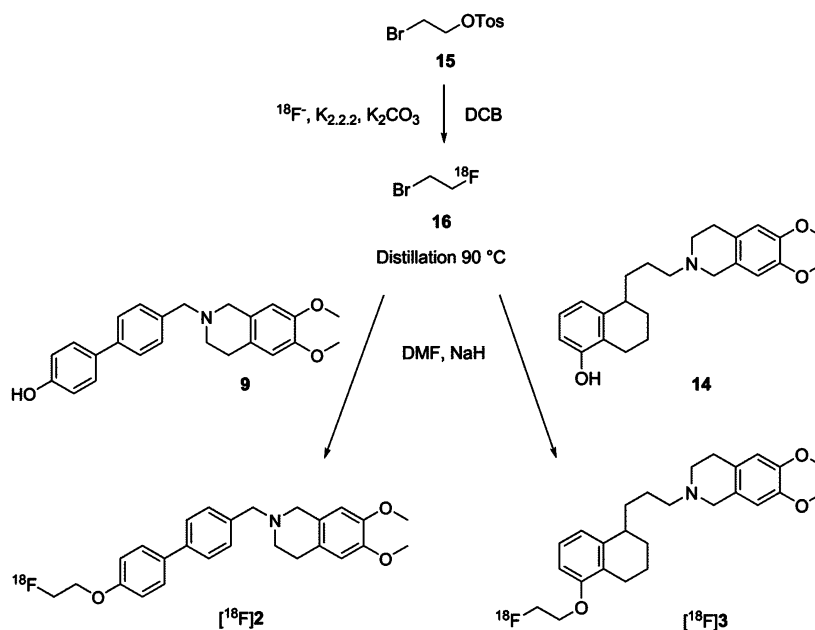
Scheme 4. Radiosynthesis of $[^{18}F]$1a

Scheme 5. Radiosynthesis of $[^{18}F]$2 and $[^{18}F]$3

Figure 1. Cerebral kinetics of the evaluated radiopharmaceuticals. Data are SUV-PET values for the entire brain, expressed as mean ± SEM (n = 3–6). Time point 0 min is the start of the scan.

and apical-basolateral directions (P_{app} BA/AB) was higher than the cutoff value of 2 for all the compounds (9.5, 7.9, and 6.1, respectively, for **1a**, **2**, and **3**) as presented in Table 1. EC_{50} values were determined in the Calcein-AM assay in Madin–

Darby Canine Kidney cells overexpressing selectively each transporter. Potency was tested also against multidrug resistance-associated protein 1 (Mrp1), which is another efflux transporter. All compounds showed high affinity toward P-gp,
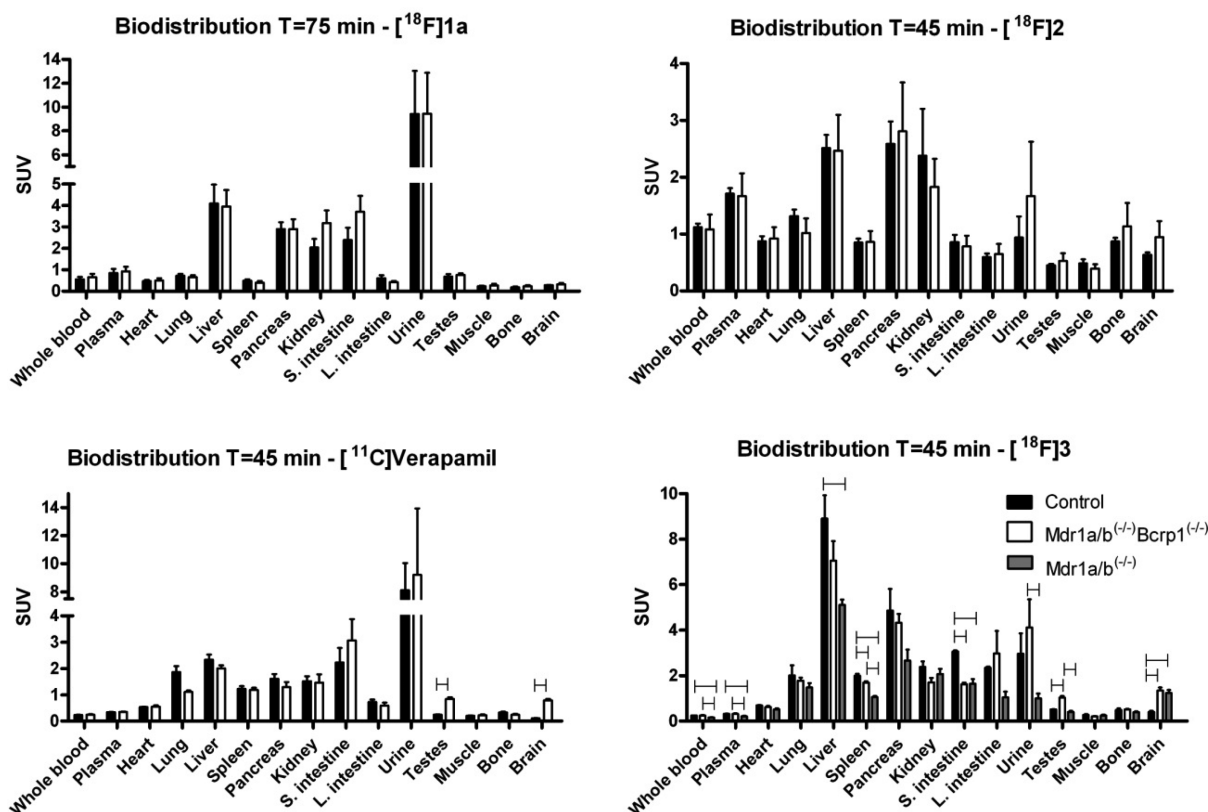
Figure 2. Biodistribution study of all the radiopharmaceuticals performed after the scans. Data are SUV expressed as mean $\pm$ SEM (n = 3−6). Statistical differences ($p < 0.05$) are marked with a capped line.

most active being **3** (EC_{50} = 0.35 μM). Only **1a** had some affinity to Bcrp (15 μM), but none of the compounds were found to have affinity to Mrp1. All the compounds activated ATPase. Based on the results from all the experiments, compounds were classified as P-gp substrates. Affinity of the compounds to sigma-1 and sigma-2 receptors was also tested at several concentrations in binding competition assays using previously published methods, as our molecules and many of the sigma ligands have a similar structure.[25,26] The half maximal inhibitory concentration IC_{50} could not be determined, and consequently neither could inhibition constant K_i, because the percentage of competition in all concentrations was less than 50%. Therefore, the percentage of competition at the highest tested concentration (1 μM) is reported in parentheses for each compound in Table 1. All compounds were found to be inactive toward sigma-1 and sigma-2 receptors, the K_i values are at least 100 times higher than the values for known sigma ligands.[27]

3.3. Radiolabeling. $[^{18}F]$**1a** was synthesized via nucleophilic aromatic substitution reaction in 90 min with a total radiochemical yield of 3.2 $\pm$ 2.6% (Scheme 4). The radiochemical purity was >96% and the specific activity 29 $\pm$ 13 GBq/μmol. Radiochemical yield (decay corrected) is calculated for the formulated product from the end of bombardment (EOB) of $[^{18}F]$fluoride. The measured log D was 2.6. $[^{18}F]$**2** and $[^{18}F]$**3** were synthesized in a two-pot method in 70−80 min (Scheme 5). They were produced with a radiochemical yield of 11 $\pm$ 4.7%. Specific activity for both radiopharmaceuticals was >100 GBq/μmol. Radiochemical purity was >98% for $[^{18}F]$**2** and >95% for $[^{18}F]$**3**. Log D value was measured as 2.9 for $[^{18}F]$**2** and 3.0 for $[^{18}F]$**3**. (R)-

$[^{11}C]$Verapamil was produced in 39 min with a radiochemical yield of 8.2 $\pm$ 4.9%, specific activity of 34 $\pm$ 16 GBq/μmol, and over 99% radiochemical purity. Radiochemical yield is calculated for the formulated product from the trapped activity of $[^{11}C]CH_4$. Log D value as measured earlier was 2.7.[28]

3.4. PET Data and Biodistribution. In the $[^{18}F]$**1a** scan the peak of activity in the brain was missed, due to the delay between radiopharmaceutical injection and start of the scan. On average, the first 7.7 min were not recorded. However, it is clear from the time−activity curves (Figure 1) that there is no difference in the brain uptake between knockout and control animals. In the biodistribution study (Figure 2), the uptake in all the organs and tissues was also similar between the strains ($p > 0.05$).

Scan time of other radiopharmaceuticals was reduced to 30 min, compared to 60 min for **1a**, as it was found to be sufficient to evaluate the cerebral uptake between the mice strains. Injections were performed directly on the microPET camera to avoid the loss of data. The cerebral kinetics of $[^{18}F]$**2** were not significantly different between the strains ($p = 0.092$). In addition, the shape of the time−activity curve was different than expected. There is no initial peak of uptake, but instead the curves are slowly rising until reaching a plateau after 10 min. In the biodistribution data, no significant difference between the strains was found. In the periphery, $[^{18}F]$**2** had only some nonspecific uptake in all the collected organs and tissues. Notable is the high uptake in plasma, which could refer to binding in plasma proteins.

$[^{18}F]$**3** had almost the same maximum uptake in the $Mdr1a/b^{(−/−)}Bcrp1^{(−/−)}$ mice as $[^{11}C]$verapamil, but the excretion from the brain was slower. Brain uptake of $[^{18}F]$**3** in the control mice
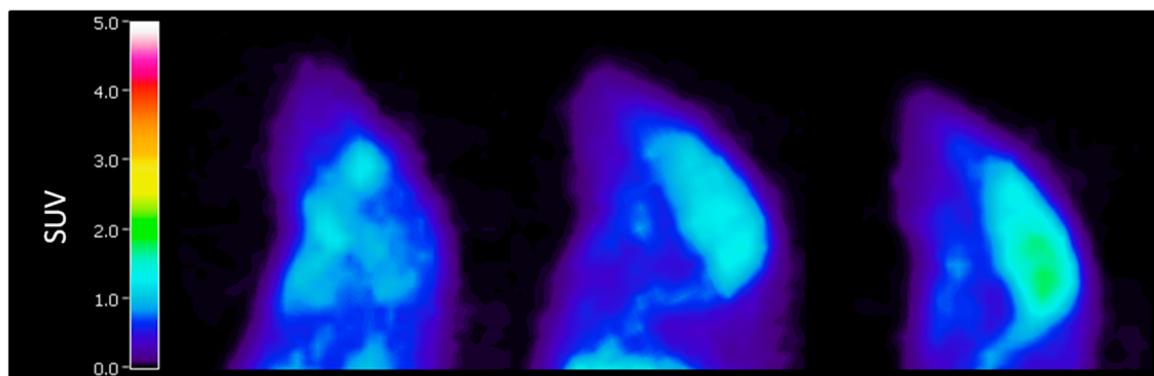
Figure 3. SUV-PET images of $[^{18}F]$**3** in control mouse (left), *Mdr1a/b*$^{(-/-)}$ mouse (middle), and *Mdr1a/b*$^{(-/-)}$*Bcrp1*$^{(-/-)}$ mouse (right), sagittal view. Vinci 4.24 software (Max Planck Institute, Cologne, Germany) was used to create the images.

was higher than for $[^{11}C]$verapamil. The area under curve (AUC) 0−30 min of $[^{11}C]$verapamil in *Mdr1a/b*$^{(-/-)}$*Bcrp1*$^{(-/-)}$ mice was 3.7-fold higher than in the control mice. In comparison with $[^{18}F]$**3**, the difference was 2-fold. Maximum knockout/control ratio with $[^{18}F]$**3** was reached in 15−20 min, whereas for $[^{11}C]$verapamil this was 5 min. There was no statistically significant difference between the $[^{18}F]$**3** uptake in *Mdr1a/b*$^{(-/-)}$*Bcrp1*$^{(-/-)}$ and *Mdr1a/b*$^{(-/-)}$ knockout mice (p = 0.316), although the SUV values are higher for *Mdr1a/b*$^{(-/-)}$*Bcrp1*$^{(-/-)}$ mice. The area under the curve of *Mdr1a/b*$^{(-/-)}$ mice constitutes about 86% of the AUC of *Mdr1a/b*$^{(-/-)}$*Bcrp1*$^{(-/-)}$mice. The examples of brain images with $[^{18}F]$**3** in each strain are displayed in Figure 3.

In the biodistribution study the uptake of $[^{11}C]$verapamil was significantly different between the strains in testes and brain at time point 45 min after injection. Statistical differences between control animals and *Mdr1a/b*$^{(-/-)}$*Bcrp1*$^{(-/-)}$ knockouts in $[^{18}F]$**3** biodistribution were found in the spleen, small intestine, testes, and brain. Between *Mdr1a/b*$^{(-/-)}$ knockouts and controls the statistical difference was found in whole blood, plasma, liver, spleen, small intestine, and brain. In contrast to the brain, the radioactivity uptake of $[^{18}F]$**3** in many P-gp containing peripheral organs was actually higher in control animals than in the knockouts.

In addition to TACs, we calculated brain-to-plasma radioactivity ratios from the biodistribution data. Therefore, the values represent only one time point after the scan (Table 2). Brain-to-plasma radioactivity ratios of $[^{18}F]$**3** suggest that radioligand is P-gp selective and is not transported by Bcrp. The difference in brain uptake between control and P-gp knockout was 4.1-fold for $[^{18}F]$**3** and 7.1-fold for $[^{11}C]$-

Table 2. Brain-to-Plasma Ratios of All Groups; Data Are Presented as Mean ± SD

groups	brain-to-plasma
$[^{11}C]$verapamil control	0.32 ± 0.1
$[^{11}C]$verapamil *Mdr1a/b*$^{(-/-)}$*Bcrp1*$^{(-/-)}$	2.3 ± 0.2
$[^{18}F]$**1a** control	0.45 ± 0.3
$[^{18}F]$**1a** *Mdr1a/b*$^{(-/-)}$*Bcrp1*$^{(-/-)}$	0.38 ± 0.1
$[^{18}F]$**2** control	0.37 ± 0.04
$[^{18}F]$**2** *Mdr1a/b*$^{(-/-)}$*Bcrp1*$^{(-/-)}$	0.54 ± 0.1
$[^{18}F]$**3** control	1.3 ± 0.2
$[^{18}F]$**3** *Mdr1a/b*$^{(-/-)}$	5.6 ± 0.8
$[^{18}F]$**3** *Mdr1a/b*$^{(-/-)}$*Bcrp1*$^{(-/-)}$	4.2 ± 1.1

verapamil. Furthermore, baseline brain uptake of $[^{18}F]$**3** was approximately 4-fold higher than for $[^{11}C]$verapamil.

3.5. Metabolism. Phase I metabolism of the nonradioactive compounds was investigated in the human liver microsomes, to study the possible metabolites and metabolism rate. Control tubes without microsomes and NADPH were included to see if the compound metabolized/degraded without them and if the microsomes were working adequately. Tubes without the test compound were analyzed to detect impurities in the chemicals or in the LC-MS system. No metabolites were observed in the control tubes with any of the tested compounds.

In the experiment performed in human liver microsomes, 60% of the intact **1a** was still present after 75 min. Decomposition of the compound caused a formation of 6,7-dimethoxy-1,2,3,4-tetrahydroisoquinoline, which was identified by MS as a primary metabolite. *In vivo* plasma samples were analyzed by radio-TLC. Majority of the metabolites were hydrophilic (>85%, R_f = 0). After 75 min, 43 ± 8.0% of the parent radiopharmaceutical was still intact. Brain metabolism data is not available.

Compound **2** was stable during the microsome study, and no metabolites were found. In the light of *in vivo* data, this could be due to the high protein binding. Only the supernatant was analyzed, but the amount of the compound in the precipitate is not known. At 45 min, 78 ± 10% of the parent $[^{18}F]$**2** was intact in the plasma and 69 ± 10% in the brain, based on the radio-TLC. All the observed metabolites were hydrophilic (R_f = 0).

Demethylation and defluoroethylation were observed for **3** in microsome incubations. After 45 min, 80% of the parent was still intact. *In vivo* at the same time point the number was 69 ± 11% in the plasma and 96 ± 0.8% in the brain. All the found metabolites were hydrophilic in the nature (R_f = 0−0.3).

In vivo $[^{11}C]$verapamil metabolite analysis was not possible due to the low activity in the plasma and brain. However, metabolism of (R)-$[^{11}C]$verapamil is known in rats.[20] According to that study, at 30 min postinjection, 47% of the parent radiopharmaceutical was intact in plasma, and at 60 min, 28%. In the brain at 30 min, 68% of the intact radiopharmaceutical was found, and at 60 min, 47%. Typical metabolites for verapamil are *O*- and *N*-demethylated compounds, as well as an *N*-dealkylated one.[20] These metabolites were found also in our microsome experiment where about 60% of the parent compound was intact at 45 min.

4. DISCUSSION

Three novel PET radiopharmaceuticals designed for imaging P-glycoprotein function were synthesized and evaluated in control and knockout mice. All of the compounds were labeled with fluorine-18 to increase their applicability. Compounds were characterized *in vitro* as substrates and were compared *in vivo* to the best known P-gp substrate [11C]verapamil.

Low radiochemical yield of [18F]**1a** (3.2%) is limiting its use. In order to improve the radiochemical yield, several different reaction temperatures and times were investigated. Microwave and microfluidic synthesis modules were also attempted to conduct the labeling, but the radiochemical yield remained low. The oxazole ring in the para-position is not a very strong activator for the nitro-group of the precursor. However, to conduct the current studies, the radiochemical yield was sufficient. Other radiopharmaceuticals were synthesized with a decent radiochemical yield of about 10%.

As expected for a substrate, [18F]**3** had higher uptake in the transporter knockout mice compared to the control mice. Uptake in the $Mdr1a/b^{(-/-)}$ knockout was a little bit lower than in the $Mdr1a/b^{(-/-)}Bcrp1^{(-/-)}$ knockout, indicating that Bcrp is involved in the transport. However, the difference in the time−activity curves was not statistically significant. *In vitro* the Bcrp affinity was not observed. The higher uptake in $Mdr1a/b^{(-/-)}Bcrp1^{(-/-)}$ mice may be due to the cooperative lack of both P-gp and Bcrp, and the pure Bcrp effect would be better investigated with $Bcrp1^{(-/-)}$ knockout. This is in contrast to (R)-[11C]verapamil, which has been found to be transported only by P-gp and not by Bcrp or Mrp1 at the BBB.[29]

Uptake in control mice was higher for [18F]**3** compared to (R)-[11C]verapamil, which could be advantageous in the cases where P-gp is overexpressed at the BBB. Upon up-regulation of P-gp, a very low PET signal can be expected, and since [18F]**3** shows higher brain uptake under normal physiological condition, its PET signal might be significantly larger than that of (R)-[11C]verapamil, assuming that the radioactivity uptake in controls in P-gp mediated.

[18F]**1a** and [18F]**2** failed to show any substrate activity for P-gp *in vivo*, although these compounds were selected from *in vitro* assays as potential candidates. Neither of them showed any difference in the brain uptake between $Mdr1a/b^{(-/-)}Bcrp1^{(-/-)}$ and control mice. In addition, [18F]**2** had high retention in plasma, which could indicate strong plasma protein binding. Compound **1a** has a 6-fold higher EC_{50} value than **3**, which could explain the poor *in vivo* results. Because **2** has an EC_{50} value in the same range as **3**, its substrate activity cannot explain this result. However, it should be noted that metabolism might play an important role *in vivo*.

Compound **3** was shown to be metabolically more stable than verapamil. *In vivo* metabolites were analyzed in plasma and brain, and *in vitro* metabolism was investigated in liver microsomes. Although liver microsomes were from a human source and *in vivo* experiments were performed in mice, metabolism rate in microsomes was quite predictable for the *in vivo* situation. More than 96% of the parent radiopharmaceutical [18F]**3** was still intact in the brain after 45 min, whereas (R)-[11C]verapamil produces much more brain entering metabolites, as was found previously in rats.[20] The *in vivo* stability of a radiopharmaceutical is of importance because PET measures only total radioactivity and cannot distinguish radioactive metabolites from the parent compound.

Both precursors of **2** and **3** (**9** and **14**) have been previously labeled with carbon-11.[23,30] The carbon-11 analogue of **2**, [11C]MC113, was characterized *in vitro* as an inhibitor but *in vivo* was weakly transported by P-gp. Uptake in the $Mdr1a/b^{(-/-)}$ mice was higher than in the control mice. In high and low P-gp expressing tumors [11C]MC113 also failed to show the difference. Change of the methyl group into a fluoroethyl in **2** affected the affinity negatively *in vivo* based on the results presented in this Article, although *in vitro* they were almost the same (MC113, 0.6 μM; **2**, 0.54 μM). Instead of affinity, a reason for this might be the better metabolic stability of [11C]MC113.

The carbon-11 analogue of [18F]**3**, [11C]MC266, was evaluated in normal rats and in rats pretreated with cyclosporine A (CsA).[23] Results were comparable to [18F]**3** studies in mice, as described in this Article. Cyclosporine A treatment increased the brain uptake of [11C]MC266 2.2-fold ($AUC_{0-60 min}$). CsA also increased the cerebral distribution volume 3-fold. Except brain, CsA treatment did not affect the radioactivity concentration in any peripheral organ.

5. CONCLUSION

In search for a new [18F]-substrate radiopharmaceutical for imaging functional changes of P-gp at the BBB, we evaluated three novel compounds: [18F]**1a**, [18F]**2**, and [18F]**3**. Due to the good metabolic stability and brain uptake, [18F]**3** is the most promising radiopharmaceutical for P-gp PET imaging. Further quantitative *in vivo* studies in rats are needed to assess the cerebral kinetics of the compound.

■ AUTHOR INFORMATION

Corresponding Author
*E-mail: g.luurtsema@umcg.nl. Tel: +31503612686.

Author Contributions
The manuscript was written through contributions of all authors. All authors have given approval to the final version of the manuscript.

Notes
The authors declare no competing financial interest.

■ ACKNOWLEDGMENTS

■ REFERENCES

(1) Giacomini, K. M.; Huang, S. Transporters in Drug Development and Clinical Pharmacology. *Clin. Pharmacol. Ther.* **2013**, *94*, 3−9.
(2) Chu, X.; Bleasby, K.; Evers, R. Species Differences in Drug Transporters and Implications for Translating Preclinical Findings to Humans. *Expert Opin. Drug Metab. Toxicol.* **2013**, *9*, 237−252.
(3) Higgins, C. F.; Linton, K. J. The ATP Switch Model for ABC Transporters. *Nat. Struct. Mol. Biol.* **2004**, *11*, 918−927.
(4) Graff, C. L.; Pollack, G. M. Drug Transport at the Blood-brain Barrier and the Choroid Plexuse. *Curr. Drug Metab.* **2004**, *5*, 95−108.
(5) Van Assema, D. M. E.; Lubberink, M.; Bauer, M.; van der Flier, W. M.; Schuit, R. C.; Windhorst, A. D.; Comans, E. F. I.; Hoetjes, N. J.; Tolboom, N.; Langer, O.; Müller, M.; Scheltens, P.; Lammertsma,

A. a; van Berckel, B. N. M. Blood-Brain Barrier P-Glycoprotein Function in Alzheimer's Disease. *Brain* **2012**, *135*, 181−189.

(6) Deo, A. K.; Borson, S.; Link, J. M.; Domino, K.; Eary, J. F.; Ke, B.; Richards, T. L.; Mankoff, D. a; Minoshima, S.; O'Sullivan, F.; Eyal, S.; Hsiao, P.; Maravilla, K.; Unadkat, J. D. Activity of P-Glycoprotein, a Β-Amyloid Transporter at the Blood-Brain Barrier, Is Compromised in Patients with Mild Alzheimer Disease. *J. Nucl. Med.* **2014**, *55*, 1106−1111.

(7) Bartels, A.; Willemsen, A. T. M.; Kortekaas, R.; de Jong, B. M.; de Vries, R.; de Klerk, O.; van Oostrom, J. C. H.; Portman, A.; Leenders, K. L. Decreased Blood-Brain Barrier P-Glycoprotein Function in the Progression of Parkinson 's Disease, PSP and MSA. *J. Neural Transm.* **2008**, *115*, 1001−1009.

(8) Langer, O.; Bauer, M.; Hammers, A.; Karch, R.; Pataraia, E.; Koepp, M. J.; Abrahim, A.; Luurtsema, G.; Brunner, M.; Sunderplassmann, R.; Zimprich, F.; Joukhadar, C.; Gentzsch, S.; Dudczak, R.; Kletter, K.; Markus, M.; Baumgartner, C. Pharmacoresistance in Epilepsy: A Pilot PET Study with the P-Glycoprotein Substrate *R*-[^{11}C]verapamil. *Epilepsia* **2007**, *48*, 1774−1784.

(9) Colabufo, N. A.; Berardi, F.; Perrone, M. G.; Capparelli, E.; Cantore, M.; Inglese, C.; Perrone, R. Substrates, Inhibitors and Activators of P-Glycoprotein: Candidates for Radiolabeling and Imaging Perspectives. *Curr. Top. Med. Chem.* **2010**, *10*, 1703−1714.

(10) Luurtsema, G.; Molthoff, C. F. M.; Windhorst, A. D.; Smit, J. W.; Keizer, H.; Boellaard, R.; Lammertsma, A. A.; Franssen, E. J. F. (*R*)- and (*S*)-[^{11}C]verapamil as PET-Tracers for Measuring P-Glycoprotein Function: In Vitro and in Vivo Evaluation. *Nucl. Med. Biol.* **2003**, *30*, 747−751.

(11) Bauer, M.; Zeitlinger, M.; Karch, R.; Matzneller, P.; Stanek, J.; Jäger, W.; Böhmdorfer, M.; Wadsak, W.; Mitterhauser, M.; Bankstahl, J. P.; Löscher, W.; Koepp, M.; Kuntner, C.; Müller, M.; Langer, O. Pgp-Mediated Interaction between (*R*)-[^{11}C]verapamil and Tariquidar at the Human Blood-Brain Barrier: A Comparison with Rat Data. *Clin. Pharmacol. Ther.* **2012**, *91*, 227−233.

(12) Bauer, M.; Karch, R.; Neumann, F.; Abrahim, A.; Wagner, C. C.; Kletter, K.; Müller, M.; Zeitlinger, M.; Langer, O. Age Dependency of Cerebral P-Gp Function Measured with (*R*)-[^{11}C]verapamil and PET. *Eur. J. Clin. Pharmacol.* **2009**, *65*, 941−946.

(13) Bankstahl, J. P.; Bankstahl, M.; Römermann, K.; Wanek, T.; Stanek, J.; Windhorst, A. D.; Fedrowitz, M.; Erker, T.; Müller, M.; Löscher, W.; Langer, O.; Kuntner, C. Tariquidar and Elacridar Are Dose-Dependently Transported by P-Glycoprotein and Bcrp at the Blood-Brain Barrier: A Small-Animal Positron Emission Tomography and in Vitro Study. *Drug Metab. Dispos.* **2013**, *41*, 754−762.

(14) Kannan, P.; Telu, S.; Shukla, S.; Ambudkar, S. V.; Pike, V. W.; Halldin, C.; Gottesman, M. M.; Innis, R. B.; Hall, M. D. The "Specific" P-Glycoprotein Inhibitor Tariquidar Is Also a Substrate and an Inhibitor for Breast Cancer Resistance Protein (BCRP/ABCG2). *ACS Chem. Neurosci.* **2011**, *2*, 82−89.

(15) Kawamura, K.; Yamasaki, T.; Konno, F.; Yui, J.; Hatori, A.; Yanamoto, K.; Wakizaka, H.; Ogawa, M.; Yoshida, Y.; Nengaki, N.; Fukumura, T.; Zhang, M.-R. Synthesis and in Vivo Evaluation of ^{18}F-Fluoroethyl GF120918 and XR9576 as Positron Emission Tomography Probes for Assessing the Function of Drug Efflux Transporters. *Bioorg. Med. Chem.* **2011**, *19*, 861−870.

(16) Dörner, B.; Kuntner, C.; Bankstahl, J. P.; Wanek, T.; Bankstahl, M.; Stanek, J.; Müllauer, J.; Bauer, F.; Mairinger, S.; Löscher, W.; Miller, D. W.; Chiba, P.; Müller, M.; Erker, T.; Langer, O. Radiosynthesis and in Vivo Evaluation of 1-[^{18}F]fluoroelacridar as a Positron Emission Tomography Tracer for P-Glycoprotein and Breast Cancer Resistance Protein. *Bioorg. Med. Chem.* **2011**, *19*, 2190−2198.

(17) Colabufo, N. A.; Berardi, F.; Perrone, M. G.; Cantore, M.; Contino, M.; Inglese, C.; Niso, M.; Perrone, R. Multi-Drug-Resistance-Reverting Agents: 2-Aryloxazole and 2-Arylthiazole Derivatives as Potent BCRP or MRP1 Inhibitors. *ChemMedChem* **2009**, *4*, 188−195.

(18) Colabufo, N. A.; Berardi, F.; Cantore, M.; Perrone, M. G.; Contino, M.; Inglese, C.; Niso, M.; Perrone, R.; Azzariti, A.; Simone, G. M.; Porcelli, L.; Paradiso, A. Small P-Gp Modulating Molecules:

SAR Studies on Tetrahydroisoquinoline Derivatives. *Bioorg. Med. Chem.* **2008**, *16*, 362−373.

(19) Wegman, T. D.; Maas, B.; Elsinga, P. H.; Vaalburg, W. An Improved Method for the Preparation of [^{11}C]verapamil. *Appl. Radiat. Isot.* **2002**, *57*, 505−507.

(20) Luurtsema, G.; Molthoff, C. F. M.; Schuit, R. C.; Windhorst, A. D.; Lammertsma, A. A.; Franssen, E. J. F. Evaluation of (*R*)-[^{11}C]verapamil as PET Tracer of P-Glycoprotein Function in the Blood-Brain Barrier: Kinetics and Metabolism in the Rat. *Nucl. Med. Biol.* **2005**, *32*, 87−93.

(21) Ma, Y.; Hof, P. R.; Grant, S. C.; Blackband, S. J.; Bennett, R.; Slatest, L.; McGuigan, M. D.; Benveniste, H. A Three-Dimensional Digital Atlas Database of the Adult C57BL/6J Mouse Brain by Magnetic Resonance Microscopy. *Neuroscience* **2005**, *135*, 1203−1215.

(22) Colabufo, N. A.; Berardi, F.; Cantore, M.; Perrone, M. G.; Contino, M.; Inglese, C.; Niso, M.; Perrone, R.; Azzariti, A.; Simone, G. M.; Paradiso, A. 4-Biphenyl and 2-Naphthyl Substituted 6,7-Dimethoxytetrahydroisoquinoline Derivatives as Potent P-Gp Modulators. *Bioorg. Med. Chem.* **2008**, *16*, 3732−3743.

(23) Van Waarde, A.; Ramakrishnan, N. K.; Rybczynska, A. A.; Elsinga, P. H.; Berardi, F.; de Jong, J. R.; Kwizera, C.; Perrone, R.; Cantore, M.; Sijbesma, J. W. A.; Dierckx, R. A.; Colabufo, N. A. Synthesis and Preclinical Evaluation of Novel PET Probes for P-Glycoprotein Function and Expression. *J. Med. Chem.* **2009**, *52*, 4524−4532.

(24) Colabufo, N. A.; Berardi, F.; Perrone, R.; Rapposelli, S.; Digiacomo, M.; Vanni, M. 2-[(3-Methoxyphenylethyl) Phenoxy]-Based ABCB1 Inhibitors: Effect of Different Basic Side-Chains on Their Biological Properties. *J. Med. Chem.* **2008**, *51*, 7602−7613.

(25) Abate, C.; Pati, M. L.; Contino, M.; Colabufo, N. A.; Perrone, R.; Niso, M.; Berardi, F. From Mixed Sigma-2 receptor/P-Glycoprotein Targeting Agents to Selective P-Glycoprotein Modulators: Small Structural Changes Address the Mechanism of Interaction at the Efflux Pump. *Eur. J. Med. Chem.* **2015**, *89*, 606−615.

(26) Matsumoto, R. R.; Bowen, W. D.; Tom, M. A.; Vo, V. N.; Truong, D. D.; Costa, B. R. Characterization of Two Novel σ Receptor Ligands: Antidystonic Effects in Rats Suggest σ Receptor Antagonism. *Eur. J. Pharmacol.* **1995**, *280*, 301−310.

(27) Van Waarde, A.; Rybczynska, A. A.; Ramakrishnan, N. K.; Ishiwata, K.; Elsinga, P. H.; Dierckx, R. A. J. O. Potential Applications for Sigma Receptor Ligands in Cancer Diagnosis and Therapy. *Biochim. Biophys. Acta* **2014**, DOI: 10.1016/j.bbamem.2014.08.022.

(28) Knutson, T. W.; Knutson, L.; Jansson, B.; Lennerna, H. The Effect of Ketoconazole on the Jejunal Permeability and CYP3A Metabolism of (R/S)-Verapamil in Humans. *J. Clin. Pharmacol.* **1999**, *48*, 180−189.

(29) Römermann, K.; Wanek, T.; Bankstahl, M.; Bankstahl, J. P.; Fedrowitz, M.; Müller, M.; Löscher, W.; Kuntner, C.; Langer, O. (*R*)-[^{11}C]verapamil Is Selectively Transported by Murine and Human P-Glycoprotein at the Blood-Brain Barrier, and Not by MRP1 and BCRP. *Nucl. Med. Biol.* **2013**, *40*, 873−878.

(30) Mairinger, S.; Wanek, T.; Kuntner, C.; Doenmez, Y.; Strommer, S.; Stanek, J.; Capparelli, E.; Chiba, P.; Müller, M.; Colabufo, N. A.; Langer, O. Synthesis and Preclinical Evaluation of the Radiolabeled P-Glycoprotein Inhibitor [^{11}C]MC113. *Nucl. Med. Biol.* **2012**, *39*, 1219−1225.

K